Characterization and modelling of the dynamic stiffness of nylon mooring rope for floating wind turbines

Hugo Thuilliez, Peter Davies, Patrice Cartraud, Mathis Feuvrie, Thomas Soulard

Characterization and modelling of the dynamic stiffness of nylon mooring rope for floating wind turbines

H. Thuilliez [a], P. Davies [b], P. Cartraud [a], M. Feuvrie [a,*], T. Soulard [a]

[a] *Nantes Universit´e, Ecole Centrale Nantes, CNRS, GeM, UMR 6183, F-44321, Nantes, France*
[b] *IFREMER Centre Bretagne, Research and Development Unit (RDT), 29280, Plouzan´e, France*

Nylon is a very promising candidate to replace steel chain moorings for Marine Renewable Energies applications like Wave Energy Converters or Floating Wind Turbine in shallow-water. However, test data for nylon ropes in a wet environment at intermediate scales are lacking in the literature except in a recent study by *Sørum et al 2022*. This article proposes a new set of experimental data on nylon subropes with a detailed test procedure. This work focuses on the dynamic stiffness of nylon mooring line and its experimental evaluation at realistic orders of mean load, load variation and frequency. We also examine the accumulated strain after successive test procedures. The experimental campaign highlights the stiffness non-linearity with respect to both the mean tension and amplitude. A simple bi-linear model taken from the work of *Huntley2016*; *Pham 2019* is considered here, and is shown to provide a good simulation of the experimental results.

1. Introduction

The number of floating wind turbines is expected to increase massively in the next decades. In order to succeed this industrial and technological challenge, the investment cost must be significantly reduced. The mooring system is responsible for 10% of floating wind turbines cost including installation cost (Katsouris and Marina, 2016; Myhr et al., 2014). Large scale installation of floating wind turbines requires cheap, reliable and correctly-sized mooring systems (Ridge et al., 2010; Depalo et al., 2022). For deep-water applications, synthetic ropes (e.g. polyester, HMPE, aramid, etc) have been widely studied and used, in order to reduce the weight of the lines, the mooring cost and peak loads compared to chains and wire (Leech et al., 2003; Banfield et al. 2005; Flory et al. 2007; Davies et al. 2011; Weller et al. 2015, Xu et al., 2021; Gordelier et al. 2015). With polyester ropes in shallow-water it is necessary either to increase the line length or to change to a more compliant mooring design, in order to obtain an acceptable tension response; very large first order motion induced forces are generated by storm waves (Pillai et al., 2022). As that solution means higher cost and footprint, nylon fiber ropes are a very attractive alternative to replace polyester ropes because of their even lower modulus and similar cost (Ridge et al., 2010).

The durability of nylon ropes under wet conditions has still to be proven, and many academic studies on this subject are ongoing. The fatigue performance can be optimized through the choice of the architecture (wire lay stranded ropes) and the type of coating (Huntley, 2016; Banfield and Ridge, 2017; Chevillotte, 2020). The lower tension levels in nylon mooring ropes could lead to a similar or increased fatigue life. In parallel, there is a need to improve the understanding of the behavior of nylon ropes under quasi-static and dynamic loading. Contrary to polyester ropes, the stress-strain response of bedded-in nylon ropes subjected to a wide range of dynamic loading is highly non-linear and hysteretic (Blaise et al. 2022). The modeling of this material is therefore much more challenging. Knowing accurately the length of the line at any moment matters because an unexpected increase in length could lead to some contact of the chain termination line with the seafloor or the platform. Such an event could negatively affect the fatigue lifetime of the line. That is why the "snap events" occurring during storms or abrupt changes in wind direction are being studied in order to quantify their influence on the dynamic stiffness and fatigue of mooring lines (Hsu et al., 2017). In addition, as shown in Pham et al. (2019), it is important to have a model that takes into account the influence of the amplitude on the dynamic stiffness, so that the tension in the mooring line can be calculated accurately under all conditions.

Based on decades of work on synthetic ropes, François & Davies (Francois et al., 2010) have proposed a model involving a separation of

* Corresponding author.
E-mail address: mathis.feuvrie@ec-nantes.fr (M. Feuvrie).

strain into several terms in line with the successive steps of a mooring analysis:

- Rope length and long-term elongation under pretension in lines (permanent loads)/model setting
- "Quasi-static stiffness" (or characteristic) to model the visco-elastic response to slow variations of mean line tension under changing weather/static analysis (equilibrium position),
- "Dynamic stiffness" to model the near-linear response to dynamic actions/dynamic response analysis (low frequency and wave frequency)

Two Joint Industry Projects ("OHP" Offloading Hawser Properties") 2007–2013, established a database of dynamic stiffness under a wide range of conditions. It was found during those projects that the François & Davies traditional approach can still be used for nylon ropes, even if the response of PA6 (Polyamide 6 or Nylon 6) ropes under cyclic loading is less linear than for polyester. The results have also shown the strong influence of water on the dynamic stiffness. The loading frequency and the loading nature (harmonic or stochastic) were considered to have little or no effect. However, this database has not been published yet.

Some results on the dynamic behavior of nylon ropes are already available. Huntley (2016) and Varney (Varney et al., 2013) have performed harmonic loading tests on nylon subropes to investigate the effect of mean load and tension amplitude on the dynamic stiffness. However, the conditions of these tests are not detailed (diameter and architecture of the subrope, nature of bedding-in, number of cycles, method for calculating the stiffness …). Weller et al. have shown the strong influence of load history on 44 mm-diameter parallel-stranded PA6 ropes, confirming the need to perform a suitable bedding-in sequence to stabilize the rope (Weller et al., 2014).

Based on the papers showing that both mean load and load amplitude have a significant effect on the dynamic stiffness of nylon ropes, in contrast to results for polyester, Pham used Huntley's results to build a bilinear model of the dynamic stiffness (Pham et al., 2019). Xu has conducted a large experimental campaign on small 3 mm-diameter ropes of several materials including nylon (Xu et al., 2021). Experimental conditions and the bedding-in procedure were precisely described. However, the effect of load amplitude was not studied, and the results can hardly be extrapolated to larger scales of nylon ropes. The accuracy of the bilinear model used with Pham's coefficients seems inconsistent, when comparing to Xu's experimental data. Indeed, the present authors used the same coefficients while nylon ropes have very different scales, architectures and bedding-in sequences. Bosman and Hooker (1999) have shown that the dynamic modulus of a polyester subrope can be extrapolated to full scale rope, but no such work has been done for nylon to date.

This bilinear model, and more widely the whole François & Davies approach, has the strong benefit of being able to be used early in the design stage thanks to its simplicity. Simultaneously, a completely different approach has been developed for many years, aiming to describe the visco-elasto-plastic behavior of synthetic ropes with one single model. This approach focuses on describing independently and mathematically the different mechanical responses of the rope rather than trying to find a general description law of the phenomenological observations. However, taking into account the load history of the ropes and the viscous effects leads to time-consuming models with many parameters. Chevillotte developed an interesting procedure based on relaxation tests and direct identification of the twelve parameters of his model (Chevillotte, 2020). Despite some effort to make this model easier to implement, Chevillotte's model is still too complex to be widely used in industrial design.

The present work proposes a new set of experimental data to describe the different parameters influencing the dynamic stiffness of wet nylon, which will allow identification of the bilinear model from the work of Huntley and Pham.

This paper is presented as follows: Section 2 presents the experimental setup and samples used for this study as well as the bedding-in procedure and the tension-driven harmonic test which imposes different values of mean load, load variation amplitude and loading frequency on each sample. The bedding-in procedure generates large permanent strain and improves the reproducibility of subsequent dynamic tests by stabilizing rheological properties of the rope. The generated strain as a function of the known maximum stress is studied. Section 3 presents the results of these tests and also shows the behavior of a single sample going through the same load regime multiple times with different recovery conditions between each test. Section 4 uses the data generated by these test results to identify the coefficients of the bilinear law for dynamic stiffness and compares them with Pham's results. Section 5 presents the conclusions and discusses the limitation of the proposed experimental campaign, together with further work that could improve our understanding of the dynamic stiffness of nylon ropes.

2. Experiments

2.1. Test bench

All tests were performed on a 30-Ton capacity uniaxial tension machine at IFREMER-Brest, operated in tension control mode.

The ropes were first immersed in tap water for at least 4 h before the test. During the test the rope was kept wet thanks to a water tank and a pump system connected to overhead sprinklers spraying the water along the central part of the rope, Fig. 1. Previous studies conducted on the same bench have shown that this configuration provides conditions close to fully immersed ropes (Weller et al., 2014).

2.2. Sensors

Displacements were measured in the central section of the rope, between the splices, by two wire displacement transducers (type ASM 1250 mm), Fig. 1. The sensors are securely bolted to the fixed tank above the water and placed at the rope level. The distance between the sensors was about 1 m. The first sensor measures the strain generated by the part of the rope before it. The second sensor does the same. By subtracting the two displacement values, we obtain the elongation of the central part of the rope. The strain used in this paper is the logarithmic strain:

$$\varepsilon_{ln} = log\left(\frac{l}{l_0}\right) \quad [1]$$

Unless otherwise specified, l_0 is here the initial length of the central part of the rope, measured after the rope is kept taut at a low tension (0.01N/tex) for the very first time. The data acquisition frequency was 4Hz. The range of displacements during harmonic cycles was from 10 to 150 mm. The accuracy of the measurement obviously depends on the amplitude of elongation that is being measured.

2.3. Samples

In this study, tests were carried out on PA6 subropes supplied by Bexco, Hamme, Belgium. The diameter of the central part of the rope between splices is around 15 mm (3-strand twisted architecture). No jacket covers the subropes. Typically, several dozens of parallel subropes are used to build the full-scale ropes like the ones that are used at sea for Floating Wind Turbine (FWT) mooring lines. Eye splices made by the supplier were used for both terminations and connected to the test machine by 100 mm diameter steel pins. The total length of the rope is about 6 m, but only the central 2-m part of the rope has a constant diameter. See Table 1 for sample specifications.

The initial length l_0 between the wire displacement attachments is measured by a measuring tape with the rope kept taut at a low tension

Fig. 1. 30 ton test bench with sprinklers and tensioned wire sensor.

Table 1
Nylon subrope measured properties.

Material	Diameter in central section (mm)	Minimum Breaking Load *MBL* (kN)	Length (m)	Wet Linear density (kg/km)	Dry Linear density *m* (kg/km)	Initial gage length at 0.01N/tex
PA6	15	70	6	186.7	120.5	1200–1855 mm

(0.01N/tex) at the start of each test. A linear density test was performed according to the Bureau Veritas (2018) *recommendations*. It is not clear if the wet value or the dry one should be used. The cable is fully immersed at sea during operation and Francois et al. (2010) have shown that the mechanical behavior of PA 6 ropes is significantly modified when wet. Indeed, nylon is very hydrophilic; to obtain meaningful data that gives a good representation of nylon's behavior in sea conditions, the rope must be kept wet for the entire duration of the test. A fully wet rope has completely different properties to those of a dry rope. This is a major difference from PET ropes, for which the variation in stiffness is much less noticeable between wet and dry samples (Bryant and Walter, 1959). However, part of the water is in the free volume of the rope and does not contribute to the mechanical response. The wet value is also less precise because an unknown mass of water is lost during the weighing procedure. Hence, the dry value of the linear density will be used in this study.

A minimum wet breaking load (MBL) of 70 kN was adopted (0.58 N/tex), following four break tests (measured break loads of 71, 71, 72 and 73 kN). Note that the tex unit is the dry linear density which is the same for each sample, 1 tex = 120.5×10^3 g/km. In order to compare subropes that differ by their architecture or diameter and to apply same stress levels, the tensions are normalized by the linear density here, rather than the MBL, because the former is more precise, considering the variation of the breaking load values between the ropes.

2.4. Bedding-in procedure

The visco-elasto-plastic behavior of synthetic fiber ropes is hard to study. To facilitate the exploitation of tension-elongation curves, operators often perform an initial bedding-in (BI) to stabilize the rheological properties of the rope. It is known that the bedding-in of synthetic ropes generates significant permanent strain and improves the reproducibility of subsequent tension-elongation curves (and thus the dynamic stiffness). Physically the changes during BI have been correlated with the decrease of the lay angle with respect to the loading axis, a greater compaction of the sub elements of the rope and maybe with a change in molecular scale (re-orientation within fibers) (Francois and Davies, 2000; Humeau, 2017). This phenomenon led certification societies to define a standard BI procedure for synthetic rope testing (Bureau Veritas, 2018; DNV-RP-E305, 2019). To the authors' knowledge, such a methodology has not been defined yet for nylon mooring ropes. Moreover, a BI that goes up to approximately 50% MBL may not be representative of the pre-stretch sequence of the rope performed at sea. If the tension seen by the rope during the first few months is too low, re-tensioning could be necessary (Weller et al., 2014)..

In this work, a bedding-in sequence was performed through creep-recovery stages (100sec creep/60sec recovery) of 0.05N/tex up to 0.30N/tex (approximately 50% of MBL). Harmonic loading at 0.12+-0.06N/tex (100 cycles at 15sec-period) completes the BI (Fig. 2). The aim is to stabilize to a cyclic permanent regime and improve the measurement reproducibility.

2.5. Harmonic dynamic test

After the BI, the rope is ready to undergo a dynamic test (Fig. 3). This test provides the dynamic stiffness values that are then introduced into the stiffness-based model described in the Introduction (Francois et al., 2010). The test is similar to the BV standard test (Bureau Veritas, 2018). Harmonic loadings were performed at 5 levels of mean load "Lm" (0.03, 0.06, 0.09, 0.12 and 0.18N/tex) and for each level of mean load, 4 amplitudes "La" are tested (0.2Lm, 0.4Lm, 0.6Lm and 0.8Lm). Finally, for every (Lm, La) pair, 100 cycles at low frequency with a period T_LF = 100sec and 100 cycles at wave frequency (T_WF = 15sec) were performed. It should be noted that ocean wave periods are usually in the 4–10s range, though in shallow water longer waves may occur. It was necessary to select a value for our study and the choice of a 15-s wave period was based on:

- the ISO recommendations for dynamic stiffness measurements (ISO 18692 Fiber ropes for offshore station-keeping - Polyester: frequency between 0.03 and 0.1 Hz)
- the desire to examine two different loading rates (15s and 100s here), and
- to be compatible with the test machine capacity (at higher loading rates and for large amplitudes the waveform was less regular, so results were less reliable).

The influence of the test frequency order between low or wave frequency will be discussed later. It should be noted that some control difficulties were encountered when trying to reproduce exactly the

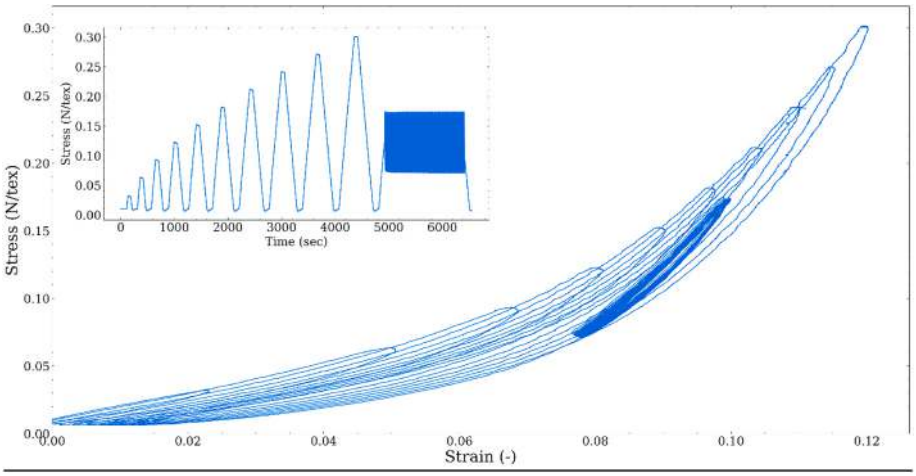

Fig. 2. Stress-strain response of a new nylon subrope subjected to a bedding-in test.

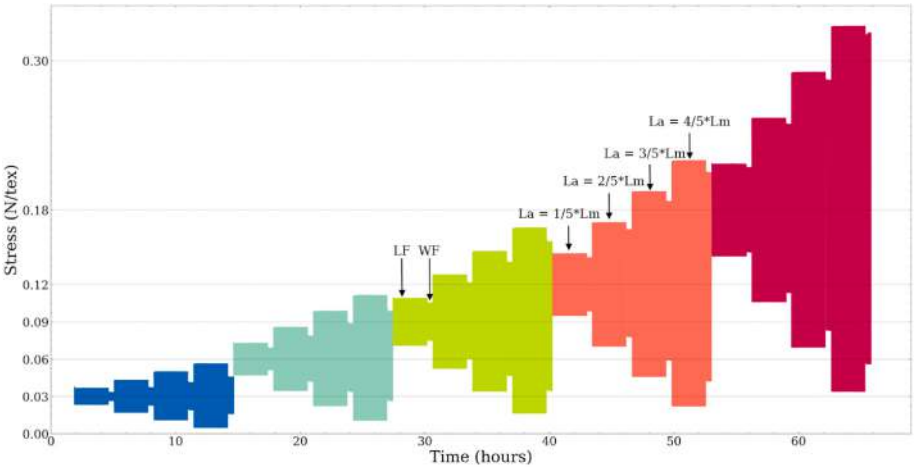

Fig. 3. Time-stress profile of the harmonic dynamic test.

tension profile for wave frequency. The tension amplitudes of wave frequency and low frequency cycles are unintentionally slightly different.

For each cycle, the axial stiffness *EA* is calculated either by linear regression or by using extreme points of the strain-tension curve (Fig. 4). Both methods give very similar results. The authors decided to use the

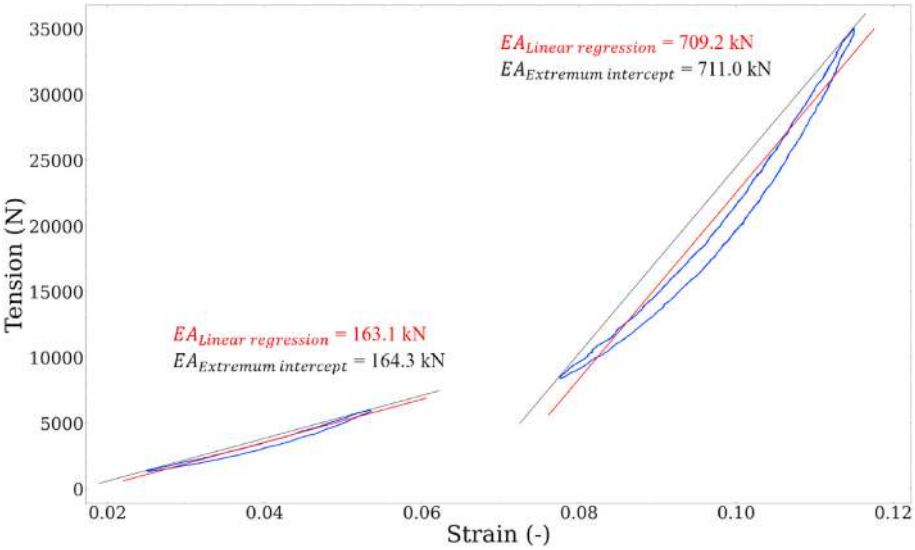

Fig. 4. Stiffness determination from the strain-tension curve. Sample 4, Lm = 0.09 and 0.18N/tex, La = 0.6Lm

linear regression method to avoid errors due to non-physical data points. Normalization of EA could be done either by the rope *MBL* or by the linear density $m = \rho.A$:

$$Krd = \frac{EA}{MBL} \quad [2]$$

$$\frac{E}{\rho} = \frac{EA}{m} \quad [3]$$

Krd is a dimensionless dynamic stiffness, $\frac{E}{\rho}$ is a dynamic modulus in N/tex. Even if Krd is more practical for users, the dimensioned dynamic modulus is preferred in this work. As the axial stiffness is normalized by the sample's linear density, it allows the resulting dynamic modulus to be easily compared to other scales of ropes or subropes.

The complex mechanical behavior of a nylon subrope cannot be reduced to a constant stiffness value. Bedded-in nylon ropes subjected to small amplitude dynamic loading show a quasi-linear stress-strain curve. However, large-amplitude cycles show a non-linear strain-stress curve and hysteresis. Thus, constant stiffness-based modeling for these loading cases is less valid.

3. Results

3.1. Bedding-in

The increasing creep/recovery stages imposed in the first step of the bedding-in generates strain, a part of which is not recovered, at least not immediately (Fig. 5). This phenomenon will also occur throughout the service life of the mooring line with each loading/unloading cycle; this will be discussed in section 3.4. A linear relation can be deduced from the BI test:

$$\varepsilon_p = \alpha * \sigma_{max} \quad [4]$$

Where ε_p is the accumulated strain generated by a rope subjected to a known maximal stress σ_{max} (N/tex). Accumulated strain is measured the same way as "classical" strain, we call it "accumulated" to emphasise the fact that strain increases a little more during each loop, as if new strain were added to existing strain. A mean coefficient $\alpha = 0.0647\ \left(\frac{N}{tex}\right)^{-1}$ was obtained from all tests performed on new 15 mm nylon subropes.

3.2. Dynamic response under low frequency or wave frequency loading

During the dynamic harmonic test, 100 cycles at low frequency are applied just before 100 cycles at wave frequency. Due to technical difficulties with the tension control on the test bench there are slightly different load variation amplitude responses between wave frequency and low frequency resulting in a lower amplitude for wave frequency (Fig. 3).

The dynamic stiffness under wave frequency cycling is a little higher than the mean stiffness for low frequency cycles (Fig. 6). This can be attributed to the lower load amplitude, which corroborates with the bilinear law detailed below.

3.3. Mean load and load amplitude influence

The experimental data clearly show that the dynamic modulus increases with increasing mean tension, and decreases as the load amplitude rises. Numerous studies have shown that mean load is the main factor affecting the dynamic stiffness of polyester ropes (Francois et al., 2010; Francois and Davies, 2008). The load amplitude is not taken into account in classical models for polyester. Previous studies have shown that dynamic stiffness of nylon ropes is strongly dependent on both mean load and load amplitude (Varney et al., 2013; Huntley, 2016).

3.3.1. Stiffness stabilization

One hundred cycles are sufficient to stabilize the dynamic modulus of the rope, except for the first amplitude of every mean tension tested (rectangular boxes in Fig. 7 below). Indeed, the loading ramp between one mean tension and a higher one is slow (0.001N/tex/sec) but cannot be considered as infinitely slow. Furthermore, the experimental results show that overall, the dynamic stiffness increases with Lm and decreases with La. However, the viscosity slows down the stiffness variation. As a result, when Lm increases (which corresponds to the 1st series of results where La varies since we have only changed the value of Lm), the dynamic stiffness increases which, in conjunction with the viscosity, leads to the damped curve we see in Fig. 6 after increasing Lm. On the other hand, when Lm is constant and La increases, the stiffness decreases, which, in conjunction with the viscosity, leads to the damped curve we see in Fig. 6 for series 2, 3 and 4 of a same Lm sequence where La increases. Even for these Lm, La pairs, a plateau seems to be reached after 100 cycles.

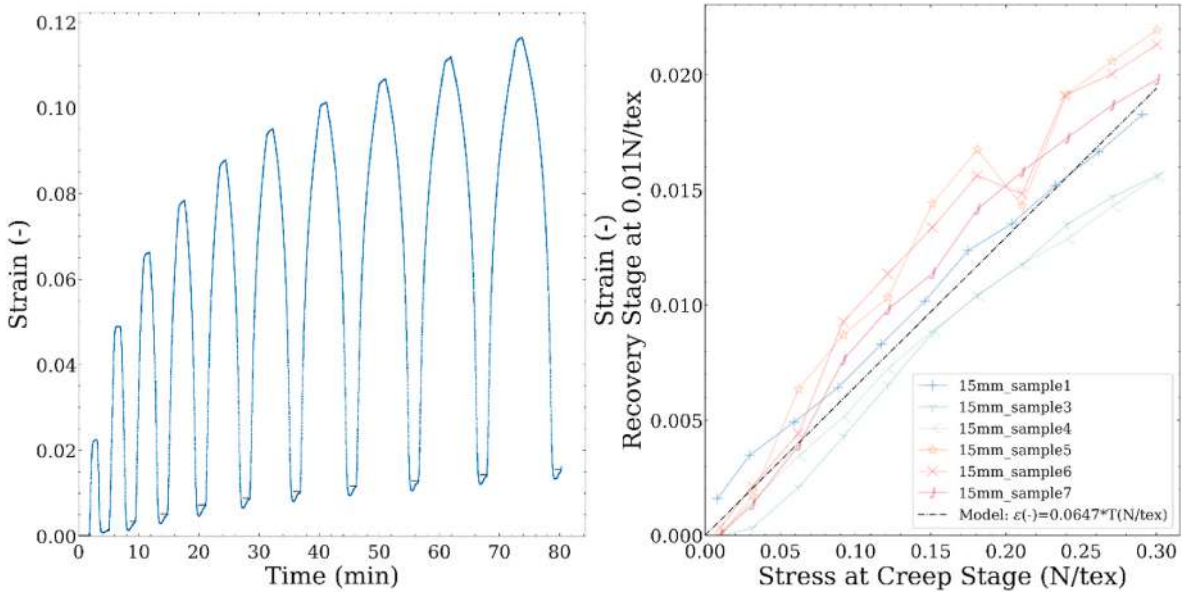

Fig. 5. Accumulated strain generated during bedding-in of 15 mm new nylon rope.

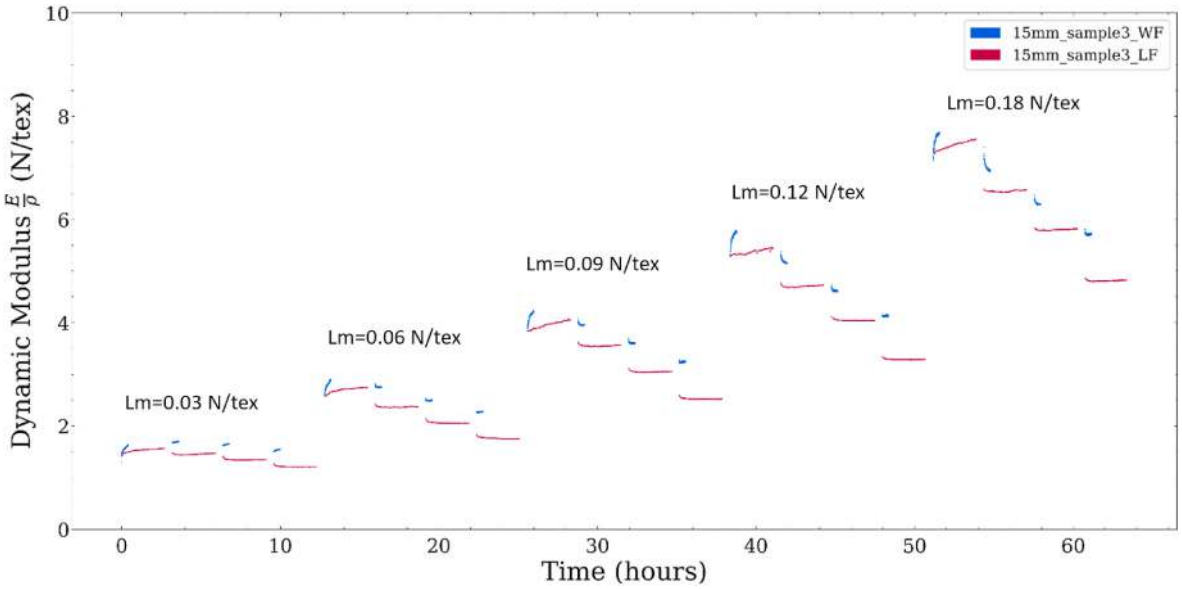

Fig. 6. Influence of loading period on dynamic modulus (the curves have been shifted horizontally to overlay both Low Frequency and Wave Frequency responses). For each of the 5 values of Lm, there are 4 different values of La: 0.2Lm, 0.4 Lm, 0.6 Lm, 0.8 Lm

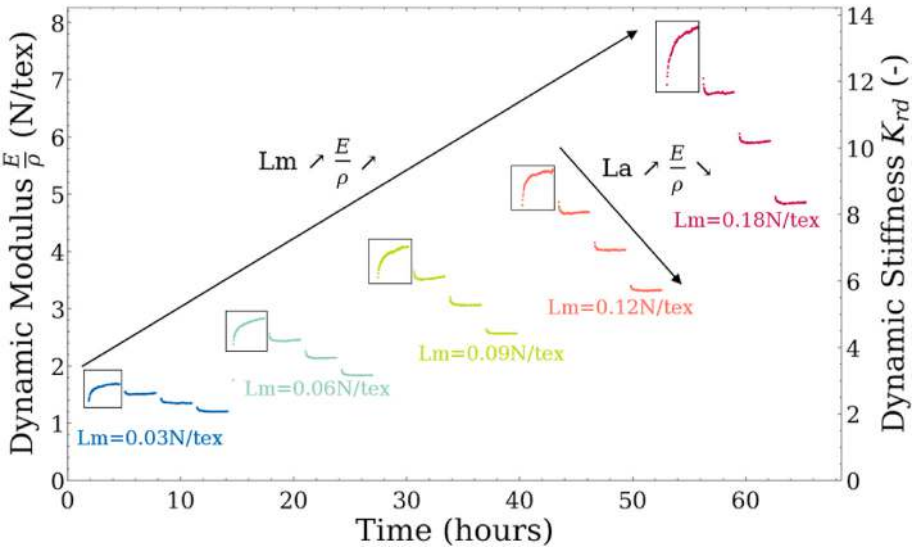

Fig. 7. Mean load and load amplitude dependency of the dynamic modulus. Sample 4, wave frequency.

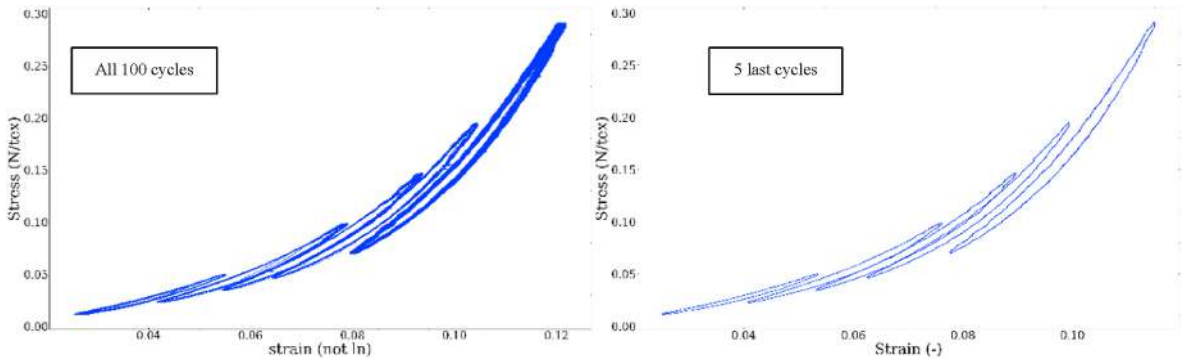

Fig. 8. Example of tension/strain curve of harmonic sequence on bedded-in sample 4 for La = 3/5*Lm at low frequency.

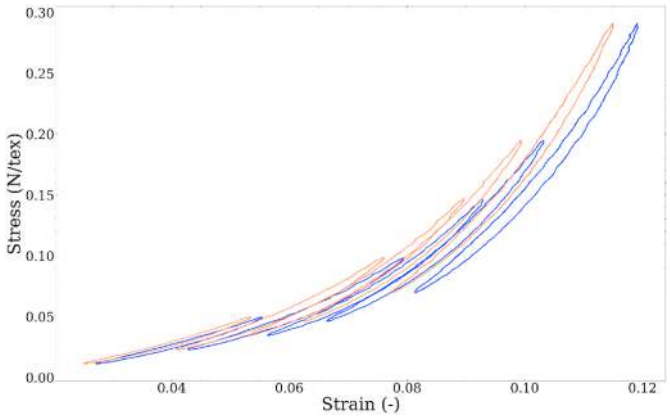

Fig. 9. Last five cycles of all dynamic tests with La = 3/5*Lm of bedded-in nylon ropes. Sample 3 (blue), sample 4 (orange).

A linear regression was applied to all points recorded during the last five cycles of each sequence to obtain the final value of each stiffness, (Fig. 8).

Fig. 9 shows the tension versus strain curves for samples 3 and 4. Apart from a small strain offset, resulting from the residual deformation after bedding-in, which is not exactly the same for each sample, the curves are close to each other, indicating a good reproducibility of the test.

3.4. Residual strain

As stated in section 2.4 the bedding-in sequence should allow a nylon rope to release the majority of the permanent strain induced by its architecture (decrease of lay angle and molecular re-orientation). The objective of this section is to observe whether the chosen BI allows the response of the subrope to be completely and permanently stabilized. The results presented in this section show that this is not completely the case. The sequence *Bedding-In + harmonic dynamic test* was repeated several times on the same 15 mm sample. Between the tests, the subrope was either kept at a very low tension (0.01N/tex) or fully unloaded for a specific time (Table 2).

The increasing creep/recovery stages of the BI generate strain, a part of which is not recovered, at least not immediately (see part 2.4.). The residual strain generated during the bedding-in is plotted on Fig. 10 as a function of the creep tension level. Unlike previous figures, the strain here is calculated with respect to the length of the rope when kept taut at 0.01N/tex at the beginning of the current sequence (and not relative to the initial length of the new rope).

- When performed on a new rope (blue, sample3A), the bedding-in generates cumulated strain as a near linear function of the maximal stress.
- After the BI and the dynamic harmonic of the test 3A, the subrope was kept taut at 0.01N/tex for 26 h. No major recovery of the cumulated strain is observed during this step. The test 3B is then performed (again with full test bedding-in and harmonic sequence). No additional strain is generated during the BI of this test. A slight recovery is even observed. The same procedure is repeated for the test 3C on the sample on which therefore 2 BI and 2 dynamic tests had already been performed. Similar results are obtained.
- After the test 3C, the rope sample was fully unloaded for 30 min before the next test, by removing the loading pin. As shown in part 3.2, a part of the cumulated strain is then recovered. The BI that follows (test 3D) generates additional residual strain. Unsurprisingly, the cumulated strain generated during this test is smaller than for a new rope.
- After the BI and the dynamic harmonic loading of the test 3D, the rope is fully unloaded for 24 h before the next test. The cumulated strain has recovered to 86% to its initial value. The BI that follows (test 3E) generates even more residual strain than that of a new rope.

Table 2
Several tests performed successively on sample 3.

Number of the test on the same 15 mm sample	Holding tension before test (N/tex)	Time on test frame before test (hours)
3A	New subrope	
3B	0.01	26
3C	0.01	14
3D	0 (fully unloaded)	0.5
3E	0 (fully unloaded)	24

Using only the last 5 stabilized cycles of each pair of parameters (Lm, La) in the dynamic test, we plot the strain-stress curves and the dynamic modulus as a function of time (Fig. 11). The strain is calculated relative to the length of the rope when kept taut at 0.01N/tex at the beginning of the current dynamic test. For example, the strain of the test *dynamic harmonic 3C* equals to $\varepsilon^{3C} = log\left(\frac{l}{l_0^{3C}}\right)$, where l_0^{3C} is the length of the rope at the end of the test *bedding-in 3C*. For visibility purposes, only the pairs (La = 1/5*Lm, Lm) are plotted in Fig. 11a.

The dynamic modulus seems slightly lower for the tests where the rope had been fully unloaded for a long time (tests 3D and 3E, Fig. 11b). That suggests that the BI performed before each dynamic test is not sufficient to fully stabilize the dynamic behavior or simply that, at this level of loading, the viscous behavior of the nylon is still far more present (but slow) than its plasticity. Also, the dynamic modulus of tests 3B and 3C are almost identical, meaning that the rope behavior does not show viscosity until the 3D test after being fully relaxed. However, this does not apply to every loading case so we cannot make a strong statement about the influence of relaxation time and tension hold on the dynamic stiffness. Further studies are needed in order to quantify that influence precisely.

4. Dynamic stiffness modeling

4.1. Bilinear model & identification procedure

As explained in the Introduction, the synthetic mooring design relies on a rope stiffness definition according to the type of mechanical stress the line is subjected to: Quasi-static stiffness for slow mean load variations under changing weather, dynamic stiffness for dynamic actions (low frequency and wave frequency). As the dynamic stiffness is known to be higher than the quasi-static stiffness for polyester ropes, the authors have focused their attention on the dynamic actions here. Moreover, this dynamic stiffness will be used for designing the rope in fatigue from its response to various sea states, computed from dedicated softwares.

Pham (Pham et al., 2019) extended the classical mean load dependent models of polyester ropes to nylon by adding a tension amplitude dependency (equation [5]). We refer to this model as the bilinear model.

$$Krd\,(-) = \frac{E.A}{MBL} = a^{MBL} * Lm^{MBL} - b^{MBL} * La^{MBL} + c^{MBL} \quad [5]$$

Where *Krd* is the non-dimensional dynamic stiffness as defined in equation [2], Lm^{MBL} and La^{MBL} are respectively the mean load and load amplitude as a percentage of MBL:

$$Lm^{MBL} = \frac{Lm}{MBL}.100 \quad [6]$$

$a^{MBL}, b^{MBL}, c^{MBL}$ are the coefficients of the model. We modify the equation in order to introduce the dynamic modulus in N/tex:

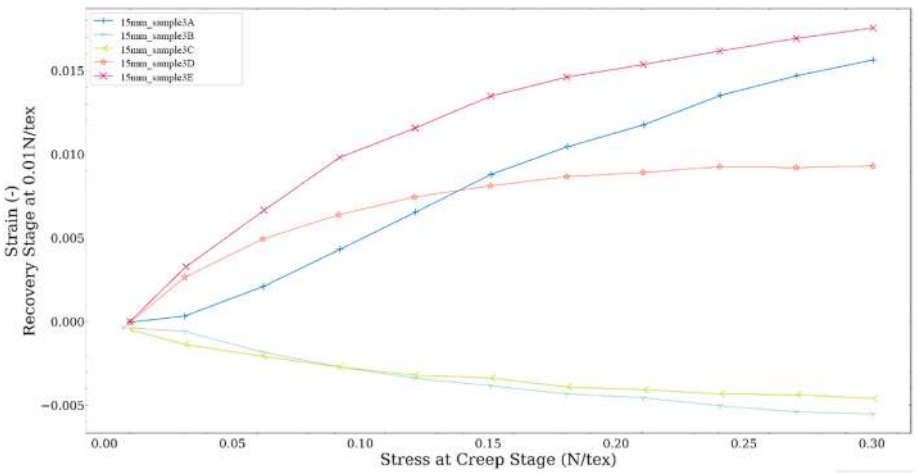

Fig. 10. Residual strain generated during the bedding-in of previously tested nylon ropes.

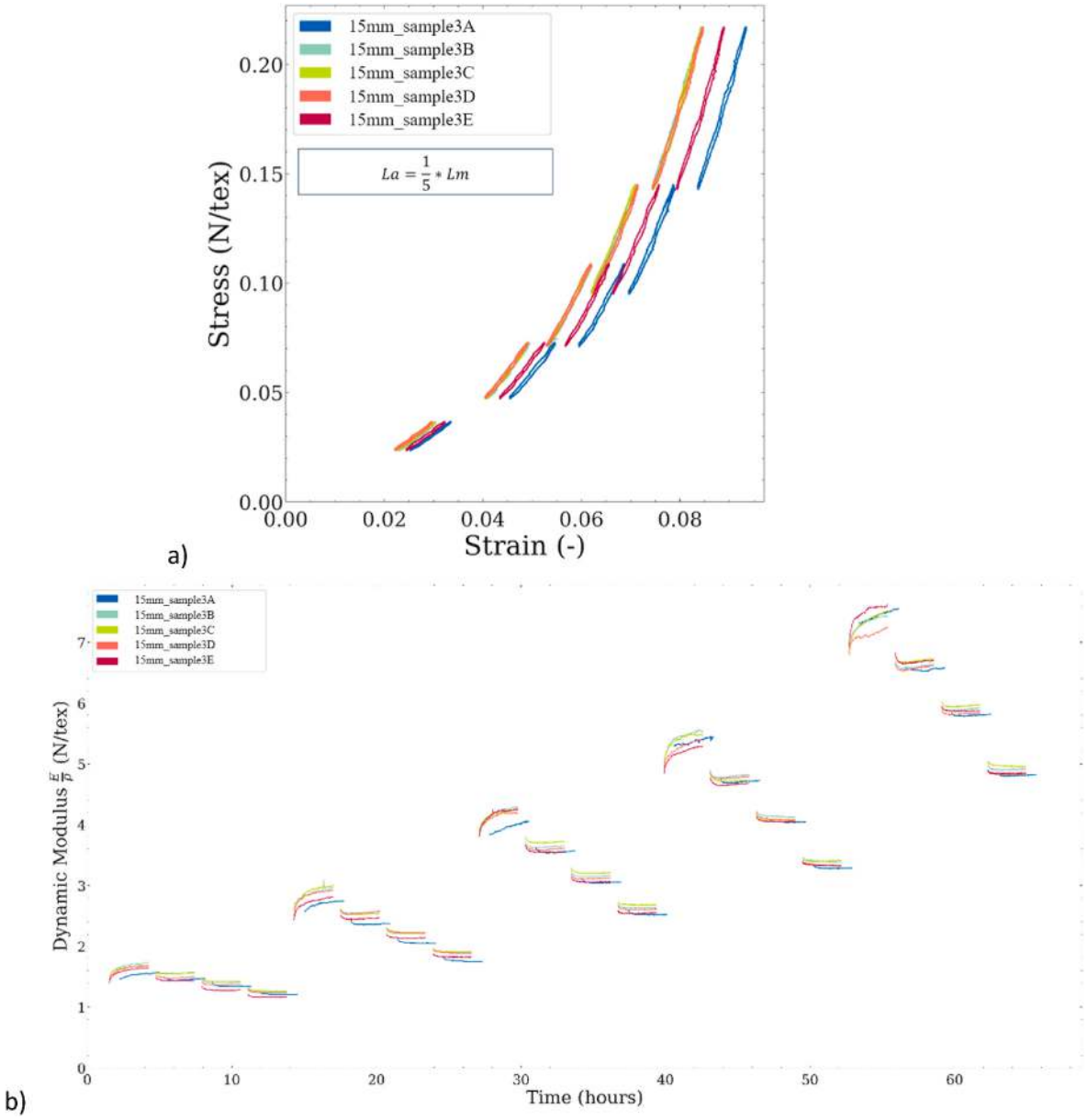

Fig. 11. Stress-strain (a) and dynamic modulus evolution (b) curves for dynamic harmonic test performed on the same nylon subrope at wave frequency.

$$\frac{E}{\rho}\left(\frac{N}{tex}\right)=\frac{E.A}{m}=a^m*Lm^m-b^m*La^m+c^m \quad [7]$$

Where Lm^m and La^m are the mean load and load amplitude normalized by the linear density m.

$$Lm^m=\frac{Lm}{m} \quad [8]$$

By replacing the expression of Lm^{MBL} and Lm^{MBL} in the equations of Krd and $\frac{E}{\rho}$ the a^m, b^m, c^m coefficients can be defined from the $a^{MBL}, b^{MBL}, c^{MBL}$ coefficients as: $a^m = 100 * a^{MBL}, b^m = 100 * b^{MBL}$ and $c^m = c^{MBL} * \frac{MBL}{m}$.

The identification of Pham's model coefficients (Table 3) was applied to Huntley's data, even though the experimental parameters are not completely known (nature of bedding-in, wetting conditions …). The present study proposes a larger experimental campaign allowing more parameters to be taken into consideration. Table 3 provides the coefficients of the bilinear model identified from the dynamic tests (harmonic or realistic) of bedded-in ropes. For the harmonic test, the experimental dynamic modulus of each (Lm, La) pair is taken as the mean dynamic modulus of the last 5 cycles. These coefficients have been obtained from the minimization of the following function:

$$func(a^m,b^m,c^m)=\sum_{i=1}^{N}\left[a^m*Lm_i^m-b^m*La_i^m+c^m-\left(\frac{E}{\rho}\right)_i\right]^2 \quad [9]$$

Where (Lm_i^m, La_i^m) is the i^{th} mean stress and stress amplitude pair tested, $\left(\frac{E}{\rho}\right)_i$ the associated experimental dynamic modulus and N is the number of pairs tested. For the harmonic test $N = 20$ which corresponds to 5 values of mean load and 4 values of load variation amplitude.

4.2. Standard deviation and correlation with the model

The bilinear model shows an excellent agreement with the experimental dynamic moduli (mean square error relative to experimental dynamic modulus around 3%). We obtain much better results than with Pham's coefficients identified on Huntley's data (Pham et al., 2019; Huntley, 2016). However, the reader should keep in mind that reducing the mechanical behavior of nylon ropes to a dynamic modulus is already a simplification.

We propose the following final coefficient values for subropes, well bedded-in at 0.30N/tex, identified from the mean of all measured stiffness values (low frequency and wave frequency) for each couple of Lm, La:

$$a^m = 46.3 b^m = 27.3 c^m = 0.501\ N/Tex \quad [10]$$

Note that the bilinear law presented here and its coefficients have been identified from all tests conducted in a chosen frequency range going from wave frequency to "low" frequency (corresponding to the frequency of the tide). These coefficients are not universal to any mooring system, since we try to predict the highly nonlinear behavior of nylon ropes using a bilinear law. They are representative of the behavior of the sample within the specific domain of tension and type of nylon rope used in this research. Furthermore, it will be shown in section 3.4 that different values of coefficients are found when considering test results obtained in other references. The small scatter existing between those two and the comparison with the bilinear law are presented in Fig. 12.

Table 3 shows that the bilinear model is able to capture very precisely the measured dynamic modulus for each test. It also presents the standard deviations of all samples differentiated for low frequency and wave frequency for each parameter of the bilinear law.

Table 4 shows that the bilinear model with its final coefficients is able to predict the dynamic modulus of each test with acceptable error (below 6%).

4.3. Limits of the harmonic dynamic test and the bilinear law

When adjusting the bilinear model on harmonic test results, the last 5 cycles (out of 100) are used to calculate the dynamic stiffness. This allows the viscous and time-dependent behavior to be stabilized, so the recent history of the rope does not influence the stiffness (for example when passing from one mean tension to a higher one). However, this choice implies an approximation, because we observe a variation of the stiffness values between the first and last cycles of each couple of parameters (mean tension Lm and tension variation amplitude La).

The present bilinear law and coefficients were compared to other behaviour description laws by Xu et al. (2021). They confirm that this model describes the nylon mooring rope behaviour well, but noted that its accuracy decreases at lower mean loads. They also proposed another equation which includes the number of loading cycles N:

$$Krd = \alpha + \beta Lm - \gamma \varepsilon_a - \delta\, exp(\kappa N) \quad [11]$$

Our results show that the stiffness is time dependent but it evolves very differently whether it is measured immediately after a large change of mean tension or just a small change of amplitude (Fig. 7). This means that the exponential term in Xu's equation is not sufficient to represent the change of stiffness with the number of cycles. We could also compare Xu's measurements of Lm, La and stiffness with the bilinear law (Equation (5)) presented earlier. We found that, using their results to identify the coefficients a, b and c of a bilinear law that would fit these results, the resulting coefficients are very different from the one presented here [10]. Indeed, the bilinear law coefficients fitted from Xu's article test results, that are normalized by MBL, are a = 0.645, b = 17.5 and c = 9.02 whereas the ones presented here, also normalized by MBL to allow comparison, are 0.463, 0.273 and 0.862. Fig. 13 shows a superposition of Xu's measures in blue, a bilinear law with coefficients identified from Xu's measures in green and a bilinear law with the coefficients proposed in the present paper (Equation (10)) in orange. It can be seen that a bilinear law can accurately capture the change of the stiffness measured by Xu, even though our proposed coefficients do not capture the non-linearity of the mean tension. This can be explained by

Table 3
Coefficients of the bilinear model identified on dynamic response of bedded-in ropes.

Coefficients	a^m (−)		b^m (−)		c^m (N/tex)		Mean squared error (%)		Coefficient of determination r^2	
Test	LF	WF	LF	WF	LF	WF	LF	WF	LF	WF
Sample 1	49.9	49.5	29.9	28.8	0.303	0.369	1.59	2.24	0.999	0.998
Sample 3A	45.9	45.8	26.6	25.7	0.391	0.467	2.65	3.18	0.997	0.995
Sample 3B	44.5	45.5	25.7	27.4	0.547	0.642	3.04	3.20	0.996	0.995
Sample 3C	45.2	47.3	25.7	28.7	0.535	0.593	2.37	2.22	0.998	0.998
Sample 3D	44.2	46.7	25.2	28.9	0.545	0.606	3.15	2.53	0.996	0.997
Sample 3E	46.2	48.0	26.6	29.5	0.397	0.489	1.91	2.32	0.999	0.998
Sample 3F	46.5	48.7	27.6	32.2	0.405	0.470	2.25	2.18	0.998	0.998
Sample 4	47.3	49.9	28.0	32.1	0.393	0.437	1.44	1.78	0.999	0.999
standard deviation	1,80	1,64	1,53	2,19	0,091	0095				
(Hong-Duc Pham et al., 2019)	39.0		21.0		1.21		24.5		0.519	

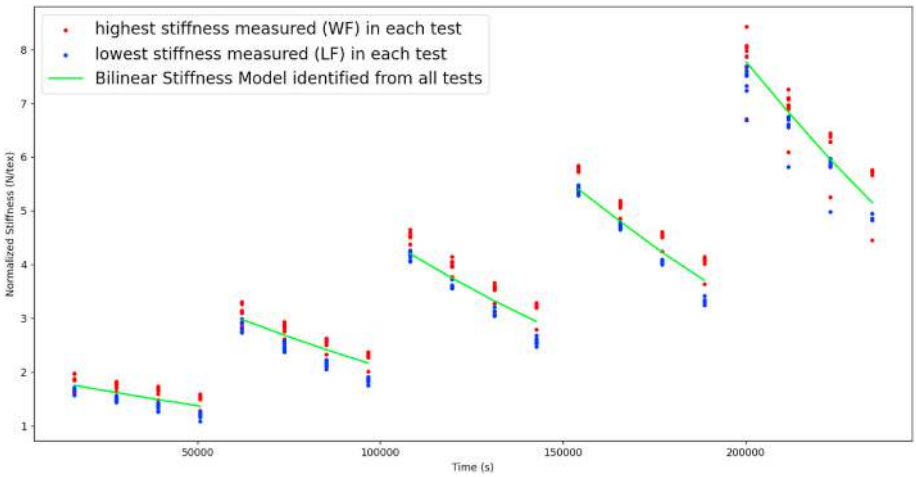

Fig. 12. Stiffness model compared with highest and lowest measured stiffness values for each 20 loading cases.

Table 4
Mean square errors of bilinear model with final coefficients.

	LF	WF
Sample1	4.99	5.60
Sample 3	3.83	3.46
Sample 3bis	3.19	4.17
Sample 3ter	2.53	5.07
Sample 3quater	3.40	4.14
Sample 3quinquies	2.95	4.20
Sample 3sexies	3.69	4.67
Sample 4	2.92	5.53

the range of La, which is very small in Xu's work; this results in a higher value for the coefficient b in order to capture the influence of La, thus reducing the influence of Lm on the model. This large difference also leads to smaller differences on the a and c parameters.

Note that the significant difference can also be explained by the different samples used in both studies. Xu et al. used small 16 strand braided ropes with an MBL of 2.7 kN but here we used much larger 3 strand twisted ropes with a 70 kN MBL.

$$Krd = \alpha + \beta Lm \quad [12]$$

We can also compare the bilinear law with the measurements of Sørum et al., 2023. They proposed a linear law for dynamic stiffness depending on mean tension:

Fig. 14 presents their measures in blue superposed with the model they proposed in red, a bilinear law where the coefficients have been fitted to their value in green and a bilinear law using the coefficients proposed here ((Equation (10)) in orange. All mean tension values are presented on the x-axis and the different La values are not shown, but their influence can be seen as a stiffness decrease as La increases. Despite a slight stiffness overestimation, there is a good correlation between the proposed bilinear law and Sørum's results. Their samples are more similar to the one used in this study than Xu's, they consist of long lay length 3-strand subropes in a complete rope with an MBL of 8682 kN. This corroborates with the fact that the bilinear law's coefficients might be more sensitive to the sample architecture than MBL and can describe a rope's behavior at higher scales. In summary, the bilinear model works for the experimental results of Huntley, Sørum, Xu and those obtained here, with 3 different sets of coefficients: one for Huntley, one for Xu, and one for Sørum and our experimental results.

During this study, we chose to normalize the dynamic modulus by the linear density of the samples measured before the tests. This allows comparisons to be made between results from samples of different sizes. Note that, due to the sample elongation, the linear density will change during the test. This raises the question of updating the linear density at each stiffness calculation, which has not been done in the present study.

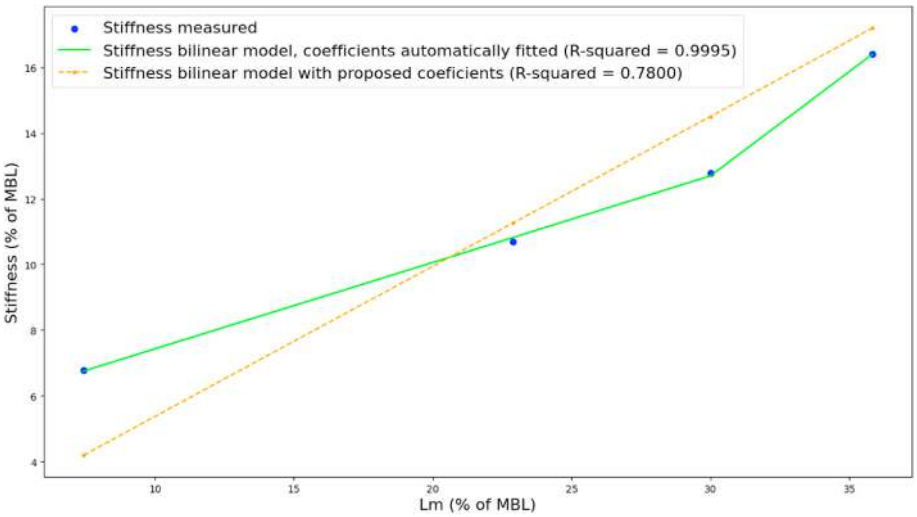

Fig. 13. Comparison of bilinear law with the data from Xu et al., (2021).

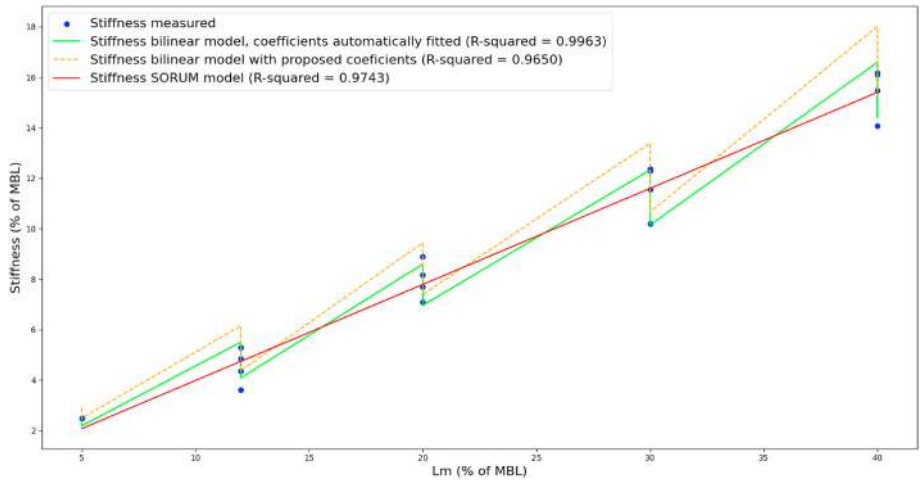

Fig. 14. Comparison of bilinear law with the data from Sørum et al., 2023.

5. Conclusion

In this study, a tension-based approach has been used to evaluate the dynamic stiffness of nylon mooring ropes. The bilinear dynamic stiffness model is used in very early design in a motion-based approach, where movements of the platform are the inputs and the tension in the mooring lines is the output. One of the aims of this work is to provide more reliable values of bilinear model coefficients for the description of stiffness in a specific domain of tension and a certain type of nylon rope, and study the influence of other parameters such as bedding-in and load frequency.

The results show a strong dependence of the dynamic stiffness on the mean tension and amplitude, and a low frequency sensitivity in the considered range. These results have been fitted using a bilinear model for dynamic stiffness, showing very good agreement between experimental data and model results. The simplicity of the model and ease of integration in commercial software will improve simulation of tension time-series and lead to more accurate prediction of extreme events and lifetime estimation. We have shown that for various conditions of mean tension and variation amplitude, a bilinear model could correlate well with the test results reported in this paper, as well as those of Sorum, Xu, and Huntley (see the Pham et al., 2019 paper for the latter). At this stage we cannot conclude on the applicability of our model's coefficients to all subrope constructions, but the three-strand twisted subrope and nylon fiber grade studied here represent the most common configuration for floating wind moorings. Further studies should be performed according to the architecture; number of yarns and fiber per strand, lay angle, type of fiber … It is recommended to perform additional trials for each new conditions of tension and rope type in order to check these coefficients. One of the samples was tested five times with the same test sequence (bedding-in and harmonic test) with different recovery times and holding tension between each sequence. The dynamic modulus was slightly lower during a test if the rope had been fully unloaded previously. Successive loading sequences induce accumulated deformation. However, a major observation was that after unloading the sample for 24 h the strain returned close to zero, meaning that the behavior responsible for the deformation was mainly viscous rather than permanent. This suggests that pre-tensioning during the installation phase may not be beneficial.

The harmonic tests allow the coefficients of the bilinear model to be easily identified but using tension time series that are not representative of the real loading of the cable in sea conditions. Future tests will be performed with more realistic loadings obtained from numerical simulations of the mooring line subjected to different sea states.

CRediT authorship contribution statement

H. Thuilliez: Conceptualization, Methodology, Data curation, Visualization, Software, Formal analysis, Investigation, Writing – original draft. **P. Davies:** Supervision, Conceptualization, Methodology, Resources, Testing, Data curation, Writing – review & editing. **P. Cartraud:** Supervision, Conceptualization, Methodology, Writing – review & editing. **M. Feuvrie:** Visualization, Investigation, Software, Formal analysis, Writing – review & editing. **T. Soulard:** Project administration, Writing – review & editing.

Declaration of competing interest

The authors declare that they have no known competing financial interests or personal relationships that could have appeared to influence the work reported in this paper.

Data availability

Data will be made available on request.

Acknowledgement

This work has received funding from the Carnot Marine Engineering Research for Sustainable, Safe and Smart Seas Institute.

References

Banfield, S., Ridge, I.M., 2017. Fatigue durability of nylon rope for permanent mooring design. In: OCEANS 2017-Aberdeen. IEEE, pp. 1–9. https://doi.org/10.1109/OCEANSE.2017.8084825.

Banfield, S.J., Casey, N.F., Nataraja, R., 2005. Durability of polyester deepwater mooring rope. In: Offshore Technology Conference. https://doi.org/10.4043/17510-MS.

Blaise, A., Bles, G., Dib, W., Shash, M., Tourabi, A., 2022. Modeling of the cyclic visco-elasto-plastic one-dimensional behavior of polyamide-based woven straps. Textil. Res. J. https://doi.org/10.1177/00405175221078533.

Bosman, R.L.M., Hooker, J., 1999 May. The elastic modulus characteristics of polyester mooring ropes. In: In *Offshore Technology Conference* (pp. OTC-10779). OTC.

Bryant, G.M., Walter, A.T., 1959. Stiffness and resiliency of wet and dry fibers as a function of temperature. Textil. Res. J. 29 (3), 211–219.

Bureau Veritas, 2018. Certification of Fibres Ropes for Deepwater Offshore Services, p. NI432.

Chevillotte, Y., 2020. Characterization of the Long-Term Mechanical Behavior and the Durability of Polyamide Mooring Ropes for Floating Wind Turbines (Doctoral Thesis, ENSTA Bretagne). https://theses.hal.science/tel-03403273.

Davies, P., Reaud, Y., Dussud, L., Woerther, P., 2011. Mechanical behaviour of HMPE and aramid fibre ropes for deep sea handling operations. Ocean Eng. 38 (17–18), 2208–2214. https://doi.org/10.1016/j.oceaneng.2011.10.010.

Depalo, F., Wang, S., Xu, S., Soares, C.G., Yang, S.H., Ringsberg, J.W., 2022. Effects of dynamic axial stiffness of elastic moorings for a wave energy converter. Ocean Eng. 251, 111132 https://doi.org/10.1016/j.oceaneng.2022.111132.

DNV-RP-E305, 2019. Design, Testing and Analysis of Offshore Fibre Ropes.
Flory, J.F., Banfield, S.J., Berryman, C., 2007. Polyester mooring lines on platforms and MODUs in deep water. In: Offshore Technology Conference. https://doi.org/10.4043/18768-MS.
Francois, M., Davies, P., 2000. Fibre rope deep water mooring: a practical model for the analysis of polyester mooring systems. Proceedings RIO2000, OSTI ID, 20456749.
Francois, M., Davies, P., 2008. Characterization of polyester mooring lines. Int. Conf. Offshore Mech. Arctic Eng. 48180, 169–177. https://doi.org/10.1115/omae2008-57136.
Francois, M., Davies, P., Grosjean, F., Legerstee, F., 2010. Modelling fiber rope load-elongation properties-Polyester and other fibers. In: Offshore Technology Conference. https://doi.org/10.4043/20846-ms.
Gordelier, T., Parish, D., Thies, P.R., Johanning, L., 2015. A novel mooring tether for highly-dynamic offshore applications; mitigating peak and fatigue loads via selectable axial stiffness. J. Mar. Sci. Eng. 3 (4), 1287–1310. https://doi.org/10.3390/jmse3041287.
Humeau, C., 2017. Contribution to the study of coupling between moisture diffusion and mechanical stress. In: High Performance Marine Materials (Doctoral thesis, Nantes).
Huntley, M.B., 2016. Fatigue and modulus characteristics of wire-lay nylon rope. In: OCEANS 2016 MTS/IEEE Monterey. IEEE, pp. 1–6. https://doi.org/10.1109/OCEANS.2016.7761501.
Hsu, W.T., Thiagarajan, K.P., Manuel, L., 2017. Extreme mooring tensions due to snap loads on a floating offshore wind turbine system. Mar. Struct. 55, 182–199.
Katsouris, G., Marina, A., 2016. Cost Modelling of Floating Wind Farms. ECN, Petten, The Netherlands. https://doi.org/10.1016/j.apor.2019.03.013.
Leech, C.M., Banfield, S.J., Overington, M.S., Lemoel, M., 2003. The prediction of cyclic load behaviour and modulus modulation for polyester and other large synthetic fiber ropes. In: Oceans 2003. Celebrating the Past... Teaming toward the Future (IEEE Cat. No. 03CH37492), 3. IEEE, pp. 1348–1352. https://doi.org/10.1109/OCEANS.2003.178056.
Myhr, A., Bjerkseter, C., Ågotnes, A., Nygaard, T.A., 2014. Levelised cost of energy for offshore floating wind turbines in a life cycle perspective. Renew. Energy 66, 714–728.
Pham, H.D., Cartraud, P., Schoefs, F., Soulard, T., Berhault, C., 2019. Dynamic modeling of nylon mooring lines for a floating wind turbine. Appl. Ocean Res. 87, 1–8.
Pillai, A.C., Gordelier, T.J., Thies, P.R., Cuthill, D., Johanning, L., 2022. Anchor loads for shallow water mooring of a 15 MW floating wind turbine—Part II: synthetic and novel mooring systems. Ocean Eng. 266, 112619 https://doi.org/10.1016/j.oceaneng.2022.112619.
Ridge, I.M.L., Banfield, S.J., Mackay, J., 2010. Nylon fibre rope moorings for wave energy converters. In: OCEANS 2010 MTS/IEEE SEATTLE. IEEE, pp. 1–10.
Sørum, S.H., Fonseca, N., Kent, M., Faria, R.P., 2023. Assessment of nylon versus polyester ropes for mooring of floating wind turbines. Ocean Eng. 278, 114339.
Varney, A.S., Taylor, R., Seelig, W., 2013. Evaluation of wire-lay nylon mooring lines in a wave energy device field trial. In: 2013 OCEANS. IEEE, San Diego, pp. 1–5. https://doi.org/10.23919/OCEANS.2013.6741077.
Weller, S.D, Davies, P., Vickers, A.W., Johanning, L., 2014. Synthetic rope responses in the context of load history: operational performance. Ocean Eng. 83, 111–124. https://doi.org/10.1016/j.oceaneng.2014.03.010. June 2014.
Weller, S.D., Johanning, L., Davies, P., Banfield, S.J., 2015. Synthetic mooring ropes for marine renewable energy applications. Renew. Energy 83, 1268–1278. https://doi.org/10.1016/j.renene.2015.03.058.
Xu, S., Wang, S., Liu, H., Zhang, Y., Li, L., Soares, C.G., 2021. Experimental evaluation of the dynamic stiffness of synthetic fibre mooring ropes. Appl. Ocean Res. 112, 102709 https://doi.org/10.1016/j.apor.2021.102709.